https://doi.org/10.5194/essd-2022-186
Preprint. Discussion started: 16 September 2022

Open Access Earth System Science Data Discussions

A new sea ice concentration product in the polar regions derived from the FengYun-3 MWRI sensors

Ying Chen[1], Xi Zhao[2], Ruibo Lei[3,1], Shengli Wu[4,5], Yue Liu[1], Pei Fan[1], Qing Ji[1], Peng Zhang[4,5], Xiaoping Pang[1†]

[1]Chinese Antarctic Center of Surveying and Mapping, Wuhan University, Wuhan, 430079, China
[2]School of Geospatial Engineering and Science, Sun Yat-Sen University & Southern Marine Science and Engineering Guangdong Laboratory, Zhuhai, China
[3]Key Laboratory for Polar Science of the MNR, Polar Research Institute of China, Shanghai, China
[4]Key Laboratory of Radiometric Calibration and Validation for Environmental Satellites, National Satellite Meteorological Center (National Center for Space Weather), China Meteorological Administration, Beijing, China
[5]Innovation Center for FengYun Meteorological Satellite (FYSIC), Beijing, China

[†]*Correspondence to*: Xiaoping Pang (pxp@whu.edu.cn)

Abstract. Sea ice concentration (SIC) is the main variable for quantifying the sea ice change in the polar regions. Continuous SIC data is very important for the studies of climate and polar marine environments. This study generates a new SIC product covering the Arctic and Antarctic from November 2010 to December 2019. It is the first long-term SIC product derived from the Microwave Radiation Imager (MWRI) sensors onboard the Chinese FengYun-3B, -3C, and -3D satellites, after a recent re-calibration of brightness temperature. We also modified the preliminary dynamic tie points Arctic Radiation and Turbulence Interaction Study Sea Ice (ASI) algorithm mainly through input TB and initial tie points. The MWRI-ASI SIC was compared to the existing ASI SIC products and validated using ship-based SIC observations. Results show that the MWRI-ASI SIC mostly coincides with the ASI SIC obtained from the Special Sensor Microwave Imager series sensors, with overall biases of -1.4 ± 1.8% in the Arctic and 0.5 ± 2.2% in the Antarctic, respectively. The overall mean absolute deviation between the MWRI-ASI SIC and ship-based SIC is 16.1% and 17.1% in the Arctic and Antarctic, respectively, which is close to the existing ASI SIC products. The trend of sea ice extent (SIE) derived from MWRI-ASI SIC closely agrees with those of the Sea Ice Index SIEs provided by OSI-SAF and NSIDC. Therefore, the MWRI-ASI SIC is comparable with other SIC products and is qualified to be integrated into long-term sea ice records. The MWRI-ASI SIC dataset is available at https://doi.pangaea.de/10.1594/PANGAEA.945188 (Chen et al., 2022).

1 Introduction

The sea ice concentration (SIC) and sea ice extent (SIE), which have been continuously and regularly provided by passive microwave (PM) remote sensing for more than four decades (Trewin et al., 2021; Lavergne et al., 2022), are crucial phenological indicators for the changes in the climate and marine environment in the polar regions. The PM SIC is the most vital data to initialize the sea ice condition for numerical modeling due to its continuous observations (Meier, 2019). The SIE in the polar regions has significant annual cycles and year-to-year variations, which are closely related to the changes in climate and ecosystem in the polar regions, and global ocean circulation, suggesting significance as a climate index on both regional and global scales (Comiso et al., 2017; Parkinson and DiGirolamo, 2021; Heil et al., 2006).

The continuous and consistent PM sea ice records are at the potential risk of breaking because spaceborne sensors are still very limited and extended service. The currently operating Special Sensor Microwave Imager Sounder (SSMIS) and Advanced Microwave Scanning Radiometer 2 (AMSR2) sensors have surpassed their design lifetime for several years (Gerland et al., 2019). The new missions for successors of these two sensors or the launch plans for other instruments, e.g., the Copernicus Imaging Microwave Radiometer (Jiménez et al., 2021) and Weather Satellite Follow–On–Microwave (Newell et al., 2020), are still in the preparation stage. The interruption of PM sea ice data would impede the tracking of the response of sea ice to climate change and the continuous applications for climate models or multidisciplinary studies in the polar regions (Witze, 2017). The Chinese instruments, the Microwave Radiation Imager (MWRI) sensors onboard the FengYun-3 (FY-3) series satellites, i.e., FY-3A, FY-3B, FY-3C, and FY-3D (Zhang et al., 2018, 2019; Xian et al., 2021), are promisingly used to provide long-term sea ice data and avoid the potential data gap (Chen et al., 2021; Zhao et al., 2022).

The SIE products derived from the PM SIC products based on various sensors or algorithms revealed biases, ranging from 0.5×10^6 to 1×10^6 km^2, or about 3% (in winter) to 20% (in summer) of the total Arctic or Antarctic SIE (Meier and Stewart, 2019). The main factors affecting the uncertainties of SIC and SIE are the sensitivities of SIC algorithms to atmospheric emission and sea ice emissivity, especially for the thin ice or the ice in the melting stage (Ivanova et al., 2015). The SIC products with higher spatial resolutions could detect finer characteristics of the ice edge but would ignore the ice having the relatively thin thickness or melting surface, resulting in the underestimation of SIE in the marginal ice zone (MIZ) (Meier and Stewart, 2019). Thus, the uncertainties of SIC and SIE are generally greater in the melting seasons than in the freezing seasons. The uncertainties of SIC and SIE are also due to the different operations to remove spurious sea ice caused by the weather effects and land spillover (Meier and Stewart, 2019; Kern et al., 2019). In addition, the inconsistency of different sensors and the drift of the sensor itself with increased operation time can increase the uncertainties of SIC and SIE (Eisenman et al., 2014). Thus, the additional backup data is beneficial to correct the products obtained from the discontinuous sensors. For example, the SSMIS data has been used as a bridge to compare and connect the Advanced Microwave Scanning Radiometer-EOS (AMSR-E) and AMSR2 estimates, which have a data gap from 2011 to 2012 (Meier and Ivanoff, 2017).

The ship-based visual observations of sea ice are the main data used for the ground validation of the satellite-based PM SIC products. To assess the performance of various algorithms for the SIC products, Spreen et al. (2008) compared the AMSR-E SICs derived from the Arctic Radiation and Turbulence Interaction Study Sea Ice (ASI), Bootstrap (BST), and enhanced NASA Team (NT2) algorithms to the ship-based SIC observations. Results indicated that the three SIC products were slightly lower than the ship-based SIC in winter but higher in summer by 10% to 12%, because the small-scale features such as leads and sparse small floes are easily ignored by the PM observations. Xie et al. (2013) compared the summer AMSR-E SIC to the ship-based SIC obtained in the Arctic Ocean and revealed that the AMSR-E SIC was overestimated in the Pack Ice Zone (PIZ) but underestimated in the MIZ. Kern et al. (2019) evaluated 10 PM SIC products using the ship-based SIC observations in the polar regions with medium SIC and revealed the SIC products derived from the BST algorithm had the lowest deviations against the ship-based SIC.

The first generation of daily SIC dataset derived from the MWRI sensors has been released by the Chinese National Satellite Meteorological Center (NSMC) in June 2011 using the NT2 algorithm, which had a considerable positive systematic deviation compared to the SIC obtained from the Interactive Multisensor Snow and Ice Mapping System, especially at the ice edge in summer (Wu and Liu, 2018). Due to low frequencies applied in the NT2 algorithm, the original resolutions of the NT2 SIC products are lower than those of the ASI SIC products, which is only use the highest frequency with high spatial resolution (Spreen et al., 2008). Zhao et al. (2022) produced a preliminary one-year Arctic SIC product derived from the FY-3D MWRI sensor using a dynamic tie points ASI algorithm, which had a smaller deviation against the AMSR2 SIC derived from the ASI algorithm compared to the Sea Ice Index SIC, OSI-430-b SIC, and AMSR2 SICs derived from the BST and NT2 algorithms.

In order to promote the application of MWRI sensors, especially to back up the existing sea ice products, this study extends the work of Zhao et al. (2022) and generates a new polar SIC product from November 2010 to December 2019. The recently re-calibrated brightness temperature (TB) of the MWRI sensors provided by NSMC (Wu et al., 2022) were used in this study to ensure the consistency of this new MWRI SIC product. The previous ASI algorithm involving dynamic tie points is modified to obtain a longer MWRI SIC product. Moreover, the MWRI-ASI SIC is compared to the existing ASI SIC products and ship-based SIC observation to test its ability as an independent dataset to complement the existing PM SIC data and identify its uncertainty in various regions and seasons. We also derive SIE from the MWRI-ASI SIC and compare it to the existing SIE products to test its ability to integrate into long-term sea ice records.

2 Data and method

2.1 Re-calibrated MWRI TB data

The MWRI sensors measure the radiation of the land, ocean, and atmosphere in conically scanning mode at five frequencies between 10 to 89 GHz at both horizontal (H) and vertical (V) polarization. The footprint size of the individual frequency ranges from 9 km at 89 GHz to 85 km at 10.65 GHz. More details of the MWRI characteristics were given in Zhao et al. (2022). Although the MWRI sensors onboard the different FY-3 satellites have consistent technical characteristics, the TB data obtained from different MWRI sensors still reveal some deviations. Therefore, Wu et al. (2022) re-calibrated the MWRI TB data using the operational algorithm, which focused on the hot load, antenna, and receiver calibration, reducing the TB deviations of different MWRI sensors.

This study used the re-calibrated level 1 swath MWRI TB data from the FY-3B, FY-3C, and FY-3D satellites, provided by the NSMC (Table 1). Due to the better performance of the FY-3D MWRI sensor than others (Wu et al., 2022), we preferentially selected the MWRI TB from the FY-3D, followed by the FY-3C and FY-3B. Considering the availability and quality of the

https://doi.org/10.5194/essd-2022-186
Preprint. Discussion started: 16 September 2022

MWRI TB from different satellites, the time coverage of the FY-3B was determined as the two periods from 12 November 2010 to 30 September 2013 and from 31 May to 10 July 2015. The FY-3C covered the periods from 1 October 2013 to 30 May 2015 and from 11 July 2015 to 31 December 2017, and the FY-3D covered two years of 2018 and 2019. The re-calibrated swath MWRI TB data at 89 GHz with V- and H-polarization were applied for the ASI algorithm, and those at 18.7, 23.8, and 36.5 GHz with V-polarization were served for the weather filters. These five channels were projected onto a polar stereographic grid true at 70 degrees with a 12.5-km spatial resolution.

Table 1. Summary of the TB, sea ice surface melt/freeze onset, SIC, and SIE datasets used in this study.

Parameter	Dataset	Source	Available period	Sensor	Algorithm	Resolution (km)
TB	MWRI TB	NSMC	11/2010 – 12/2019	MWRI	-	12.5
Melt/freeze	Melt/freeze onset	GESR	2011 – 2019	SSM/I, SSMIS	PMA	25
SIC	SSMI-ASI	Hamburg Uni.	11/2010 – 12/2019	SSM/I, SSMIS	ASI	12.5
	AMSR-ASI	Bremen Uni.	11/2010 – 10/2011 07/2012 – 12/2019	AMSR-E AMSR2	ASI	6.25
SIE	SSMI-BST	NSIDC	11/1978 – 12/2019	SMMR, SSM/I, SSMIS	BST	25
	SSMI-NT	NSIDC	11/1978 – 12/2019	SMMR, SSM/I, SSMIS	NT	25
	Sea Ice Index	NSIDC	11/1978 – 12/2019	SMMR, SSM/I, SSMIS	revised NT	25
	OSI-SAF	OSI-SAF	11/1978 – 12/2019	SMMR, SSM/I, SSMIS	Bristol & BST	25

2.2 Existing ASI SIC products

Two daily SIC products using the ASI algorithm in the polar regions were used as comparative data in this study (Table 1). One is available from the Integrated Climate Data Center (ICDC) of the University of Hamburg, which is derived from the Special Sensor Microwave Imager series sensors projected onto a 12.5-km polar stereographic grid (SSMI-ASI) (Kern et al., 2020). The other is derived from the Advanced Microwave Scanning Radiometer series sensors projected onto a 6.25-km polar stereographic grid (version 5.4, AMSR-ASI) produced by the Institute of Environmental Physics (IUP) of the University of Bremen (Melsheimer and Spreen, 2020). For comparison during the overlap periods with the MWRI data, we used the SSMI-ASI SIC from November 2010 to December 2019, the AMSR-E ASI SIC from November 2010 to October 2011, and the AMSR2 ASI SIC from July 2012 to December 2019, respectively. Comparisons of the daily SICs and SIEs (SIC > 15%) derived from the MWRI-ASI, SSMI-ASI, and AMSR-ASI were performed at their native spatial resolutions.

To evaluate differences in the uncertainties of SIC between the melting and freezing periods, we used the data of Arctic sea ice surface melt or freeze onset to define the ice melting and freezing periods, which (version 371s, Table 1) is available from the Goddard Earth Science Research (https://earth.gsfc.nasa.gov/index.php/cryo/data). This data is obtained from the SSMI series sensors using the passive microwave algorithm (PMA) projected onto a 25-km polar stereographic grid, which includes the onsets of the early melt, melt, freeze, and late freeze for the sea ice surface (Markus et al., 2009). We resampled the three ASI SIC products onto a 25-km grid to combine with this data.

To assess the observation ability of different SIC products in the MIZ, where the accuracy of PM SIC is generally low, the monthly MIZ SIE and MIZ SIE fraction (the ratio between the MIZ SIE and the total SIE) obtained from the three ASI SIC products were compared. We resampled the AMSR-ASI SIC onto a 12.5-km grid corresponding to the MWRI-ASI SIC and SSMI-ASI SIC to compare the SIC during the entire overlap periods, as well as the winter (Arctic: December – May, Antarctic: June – November) and summer months (Arctic: June – November, Antarctic: December – May), respectively. To evaluate the uncertainties of SIC under different SIC scenarios, we divided SIC into three levels: low SIC (15–30%), medium SIC (30–70%), and high SIC (70–100%), and calculated the SIC differences among the ASI SIC products within each SIC level.

2.3 Existing monthly SIE products

This study used four products of monthly SIE in the polar regions from November 1978 to December 2019 (Table 1), which are all derived from SIC products at a 25-km grid resolution obtained from the SSMI series sensors. The National Snow and Ice Data Center (NSIDC) provides the SIE products using the BST and NASA Team algorithms (SSMI-BST and SSMI-NT) (Stroeve and Meier, 2018), as well as the SIE product derived from the Sea Ice Index SIC product (version 3) (Fetterer et al., 2017). The fourth SIE product is derived from the SIC product developed by the Ocean and Sea Ice Satellite Application Facility Norwegian Meteorological Institute (version 2, OSI-SAF) (Lavergne et al., 2020).

The differences between the MWRI-ASI SIE and four existing SIE products were quantified during their entire overlap periods, as well as the winter and summer months. The 2010–2019 trends of the MWRI-ASI SIE and four existing SIE products were compared. Moreover, to test the capability of the MWRI-ASI SIE as a backup, we performed an analysis of combined SIE trends. The 40-year (1979 to 2019) trends combining the four existing SIE products from January 1979 to November 2010 and MWRI-ASI SIE from December 2010 to December 2019 were compared to the original trends derived from the four existing SIE products.

2.4 Modified ASI dynamic tie points algorithm

In the previous study (Zhao et al., 2022), a TB bias-correction was performed to reduce the biases between daily MWRI TB and AMSR2 TB. An ASI algorithm involving daily dynamic tie points was applied in the Arctic. The tie points of AMSR series were used as the initial tie points, and the daily dynamic tie points were generated according to the initial SIC, locations, and time sliding window. Two weather filters and a monthly maximum ice extent mask were utilized to remove the spurious sea ice. More details about the dynamic tie points ASI algorithm were given in Zhao et al. (2022), and the details about the ASI algorithm can be referred to Kaleschke et al. (2001) and Spreen et al. (2008).

To obtain a longer dataset of MWRI SIC and optimize the estimation procedures, this study modified the previous algorithm from the five aspects (Table 2). Using daily TB, as that used in Zhao et al. (2022), would dilute the atmospheric signal due to the nonlinear atmospheric influence on the TB (Comiso et al., 2003). Thus, this study used the re-calibrated swath MWRI TB to calculate SIC and grided the swath SIC into daily SIC.

https://doi.org/10.5194/essd-2022-186
Preprint. Discussion started: 16 September 2022

Table 2. Differences in parameters or operations between the previous and modified algorithms.

Parameter/operation	Previous algorithm	Modified algorithm
input TB	daily MWRI TB bias-corrected to daily AMSR2 TB	swath re-calibrated MWRI TB
swath into daily	swath TB into daily TB	swath SIC into daily SIC
initial tie points	P_1 =11.7 K, P_0 = 47 K (Arctic)	P_1 =7.1 K, P_0 = 50.3 K (Arctic) P_1 =7.3 K, P_0 = 55.9 K (Antarctic)
dynamic tie points (Antarctic)	-	P_1: initial SIC larger than 95% within the monthly minimum ice extent, 100 km away from the coast. P_0: initial SIC within [-10%, 10%], between 200 and 350 km away from the monthly ice edge, 100 km away from the coast.
weather filters	GR(36.5/18.7): 0.045; GR(23.8/18.7): 0.04	GR(36.5/18.7): 0.05; GR(23.8/18.7): 0.045

Different from using the tie points of AMSR series as initial tie points in Zhao et al. (2022), this study proposed a new operation to generate the initial tie points. We tested the sea ice tie points (P_1) from 6.0 to 12.0 K and the open water tie points (P_0) from 47.0 to 57.0 K with an interval of 0.1 K. Based on these 6000 pairs of tie points, the swath MWRI SIC was calculated from the swath TB using the ASI algorithm and then averaged into daily SIC. We used daily SSMI-ASI SIC in 2018 as the referential SIC and computed the daily average of the MWRI-ASI SIC and SSMI-ASI SIC (SIC > 15%). Then, the linear regression was conducted between the daily average MWRI-ASI SIC and referential SSMI-ASI SIC. We selected one pair of tie points as initial tie points by satisfying requirements with the slope closer to 1, intercept closer to 0, and relatively low standard deviation (Std) among the 6000 samples. According to the above procedures, the initial P_1 were defined as 7.1 and 7.3 K, and the P_0 were determined as 50.3 and 55.9 K in the Arctic and Antarctic, respectively. This parameterization of P_1 and P_0 can effectively reduce the differences between the initial MWRI SIC and referential SSMI SIC.

As the Arctic dynamic tie points proposed in Zhao et al. (2022), this study also generated the Antarctic dynamic tie points. The conditions of sea ice tie-point samples are defined as follows: the initial SICs of grids are larger than 95%, and the grids are within the monthly minimum ice extent and 100 km away from the coast. The conditions of open water tie-point samples are defined as follows: the initial SICs of grids fall within the range [-10%, 10%], and the grids are away from the monthly ice edge by 200–350 km and away from the coast by 100 km.

The thresholds of the weather filters GR(36.5/18.7) and GR(23.8/18.7) were determined as 0.045 and 0.04 by Zhao et al. (2022), respectively, as the AMSR series sensors. In this study, we chose 0.05 and 0.045 as thresholds of GR(36.5/18.7) and GR(23.8/18.7), respectively, as the SSMI series sensors, which can generally remove the weather effects (Gloersen and Cavalieri, 1986; Cavalieri et al., 1995). Here, the GR is defined as the TB difference with V-polarization between high and low frequencies against to the sum of these two TB.

2.5 Ship-based observation data

The ship-based observations of sea ice follow the protocols of the Ice Watch/Arctic Ship-based Sea-Ice Standardization (Ice Watch/ASSIST) (Hutchings et al., 2019) in the Arctic and of the Antarctic Sea Ice Processes and Climate (ASPeCt) (Worby and Allison, 1999) in the Antarctic. The two protocols have the same observation principle for SIC, and their main difference is the description of the surface properties of sea ice, such as the quantitative description of the melt pond coverage for Arctic sea ice by the Ice Watch/ASSIST. To validate the accuracy of the MWRI-ASI SIC, we collected the observational SIC from various ship-based measurement programs of the Chinese National Arctic and Antarctic Research Expedition (CHINARE) conducted by the Polar Research Institute of China (Lei et al., 2017) and a standardized ship-based observation dataset (ESA-SICCI) produced by Kern (2019), as well as those available in the IceWatch (https://icewatch.met.no/cruises) and PANGAEA databases (https://www.pangaea.de).

A total of 8887 and 3882 samples of ship-based observations in the Arctic and Antarctic, respectively, obtained from December 2010 to November 2019 were used here. Among them, 10726 and 2043 samples were obtained from the summer and winter months, respectively. We projected the ship-based SIC onto the polar stereographic grid and computed the average of the ship-based samples obtained in one calendar day within one polar stereographic grid corresponding to the PM SIC sample. A total of 5230, 5508, and 6169 samples of the ship-based SIC corresponding to the MWRI-ASI, SSMI-ASI, and AMSR-ASI products were used in the Arctic, respectively, about 88% (12%) of which were obtained from the summer (winter) months. In the Antarctic, we collected 2599, 2613, and 2979 ship-based SIC samples corresponding to the MWRI-ASI, SSMI-ASI, and AMSR-ASI products, respectively, about 73% (27%) of which were obtained from the summer (winter) months.

We compared the three ASI SIC products to the ship-based SIC by calculating the bias, mean absolute deviation (MAD), root mean standard deviation (RMSD), and correlation coefficient (*R*) during the entire overlap periods, as well as the summer and winter months separately, at their native spatial resolutions. To evaluate the impact of sea ice conditions on the accuracy of SIC, we divided SIC as low (15–30%), medium (30–70%), and high (70–100%) levels.

3 Results

3.1 Comparisons of the ASI SIC products

All the three ASI SIC products reveal similar variation patterns in daily SIC and SIE (Fig. 1), with *R*s between each pair of products larger than 0.95 ($P<0.01$). The MWRI-ASI SIC is much closer to the SSMI-ASI SIC with overall biases of -1.4% and 0.5% in the Arctic and Antarctic, respectively, compared to the AMSR-ASI SIC. Both the MWRI-ASI SIC and SSMI-ASI SIC are lower than the AMSR-ASI SIC by about 5% in the bipolar regions. The MADs of SIE between the MWRI-ASI and SSMI-ASI are lower than those between the MWRI-ASI and AMSR-ASI by 0.2×106 km2 (or 2% of the mean total SIE) in the bipolar regions. Compared to the AMSR-ASI, the relatively small differences in SIC and SIE of the MWRI-ASI against the SSMI-ASI is likely because the initial tie points computation of the MWRI-ASI SIC was referred to the SSMI-ASI SIC.

https://doi.org/10.5194/essd-2022-186
Preprint. Discussion started: 16 September 2022

Open Access Earth System Science Data Discussions

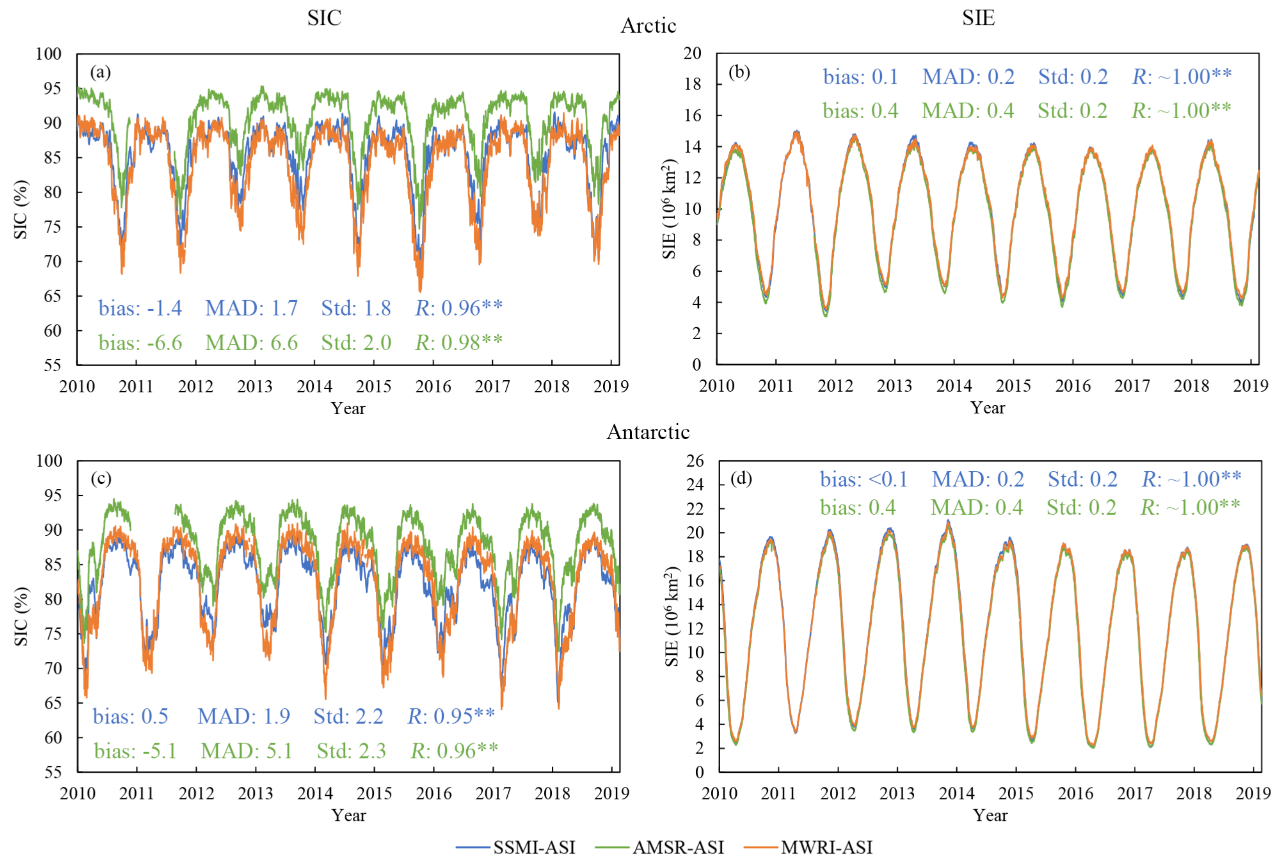

Figure 1: Daily average SIC and daily SIE from November 2010 to December 2019. Also shown are the differences in SIC and SIE between the MWRI-ASI and SSMI-ASI (blue number) and between the MWRI-ASI and AMSR-ASI (green number). The statistically significant at 95% and 99% confidence levels are marked by * and **, respectively, and those below 95% confidence level are not marked, the same below.

Compared to the total SIE, the MADs of MIZ SIE between the MWRI-ASI and SSMI-ASI increase by 0.04×10^6 and 0.1×10^6 km^2, and those between the MWRI-ASI and AMSR-ASI increase by 0.5×10^6 and 0.4×10^6 km^2 in the Arctic and Antarctic, respectively (Fig. 2). It suggests that the deviations of different SIC products increase significantly in the MIZ compared to the total ice region. Seasonally, the MWRI-ASI MIZ SIE reveals the smallest deviation against the SSMI-ASI MIZ SIE in March for the bipolar regions. However, the influence regime is different between the Arctic and Antarctic. In the Arctic, fewer spurious ice along the coast caused by land spillover is introduced into the MIZ SIE estimation in March, when the SIE reaches the maximum, reducing the deviation between two SIEs. In the Antarctic, lower MWRI-ASI MIZ SIE is exactly compensated by the spurious ice caused by land spillover and weather effects in March, leading to a near-zero bias between two SIEs. In the bipolar regions, the differences in MIZ SIE between the MWRI-ASI and AMSR-ASI are lower in winter than in summer when the MIZ SIE fraction is higher. The MIZ SIEs obtained from the MWRI-ASI SIC and SSMI-ASI SIC are larger than that obtained from the AMSR-ASI SIC, because lower grid resolutions of the MWRI-ASI and SSMI-ASI lead to

https://doi.org/10.5194/essd-2022-186
Preprint. Discussion started: 16 September 2022

Open Access Earth System Science Data Discussions

smearing at the ice edge and overestimation of MIZ SIE. Moreover, the MIZ SIE fraction of the AMSR-ASI is lower than those of the MWRI-ASI and SSMI-ASI, because the total AMSR-ASI SIC is relatively high (Fig. 1) and more grids at the boundary between the MIZ and PIZ have been identified as the PIZ by the AMSR-ASI compared to the MWRI-ASI and SSMI-ASI.

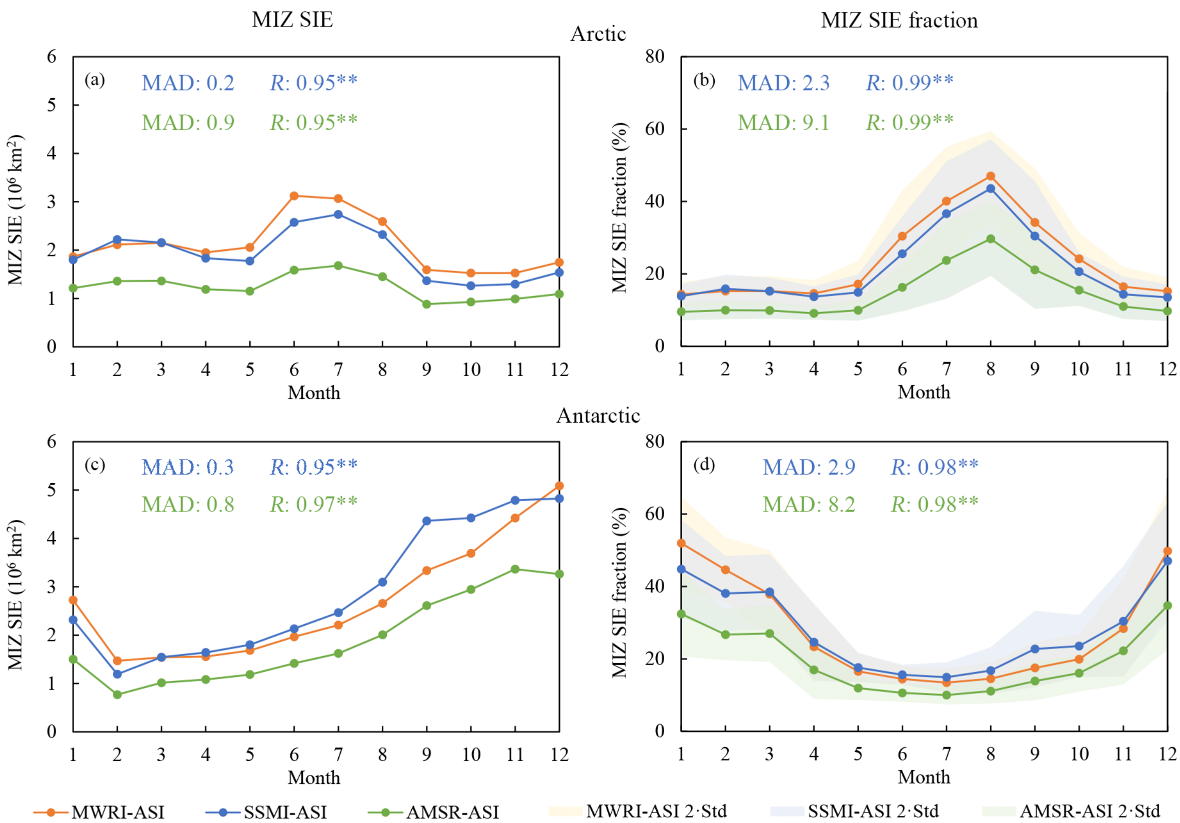

Figure 2: Monthly MIZ SIE and MIZ SIE fraction from November 2010 to December 2019. Also shown are the differences in MIZ SIE and MIZ SIE fraction between the MWRI-ASI and SSMI-ASI (blue number) and between the MWRI-ASI and AMSR-ASI (green number). The shades present the 2 Stds from the monthly MIZ SIE fraction.

Spatially, the MWRI-ASI SIC is slightly smaller than the SSMI-ASI SIC in the PIZ in the Arctic, while larger along the coastline and ice edge (Fig. 3), as the MWRI-ASI has more residual ice caused by land spillover and weather effects compared to the SSMI-ASI. In the Antarctic, the MWRI-ASI SIC is generally higher than the SSMI-ASI SIC. Compared to the AMSR-ASI SIC, the MWRI-ASI SIC is underestimated in the pan Arctic Ocean and in the PIZ in the Antarctic, while overestimated at the ice edge in the Antarctic. Note that the apparent stripes of SIC differences between the MWRI-ASI and SSMI-ASI are located at the low latitude regions in the bipolar regions (Fig. 3a, 3b, 3g, 3h), which are due to the raw stripes of the SSMI-ASI SIC.

https://doi.org/10.5194/essd-2022-186
Preprint. Discussion started: 16 September 2022

Open Access Earth System Science Data Discussions

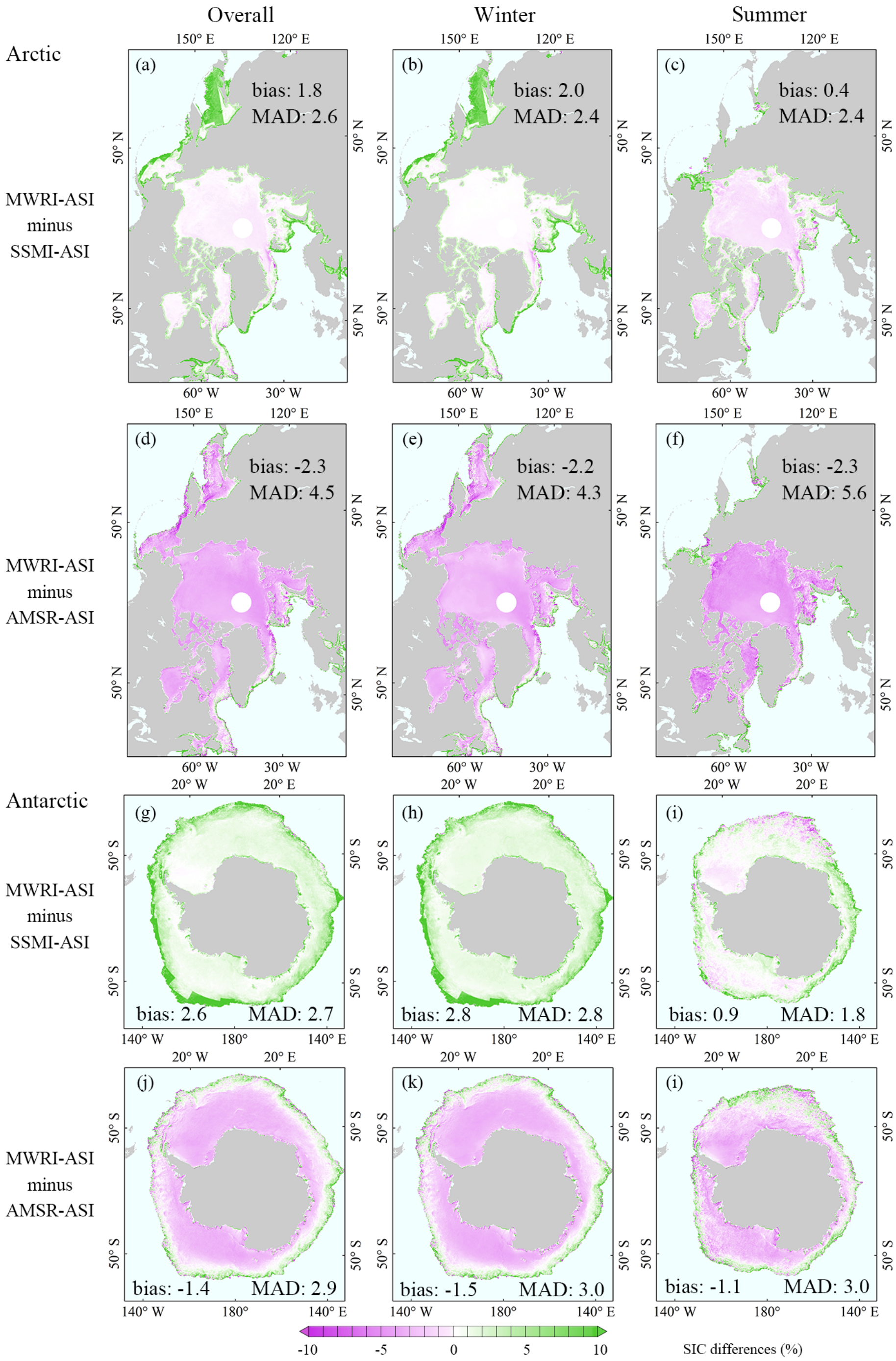

Figure 3: SIC differences between the MWRI-ASI and SSMI-ASI and between the MWRI-ASI and AMSR-ASI during the entire overlap periods, as well as the winter and the summer months from November 2010 to December 2019. The grey is land, and the light blue is open water.

https://doi.org/10.5194/essd-2022-186
Preprint. Discussion started: 16 September 2022

Open Access Earth System Science Data Discussions

In the Arctic and Antarctic, the lowest SIC differences both appear in the region with high SIC (70–100%) (Fig. 4), with mean MAD of 3.6% between the MWRI-ASI and SSMI-ASI and of 5.2% between the MWRI-ASI and AMSR-ASI, respectively. The largest MAD (15.4%) between the MWRI-ASI SIC and SSMI-ASI SIC is identified in the region with low SIC (15–30%), and the MAD between the MWRI-ASI SIC and AMSR-ASI SIC is the highest (16%) in the region with medium SIC (30–70%). Thus, the differences among the ASI SIC products are smaller in the regions of high SIC than in the regions with low or medium SIC.

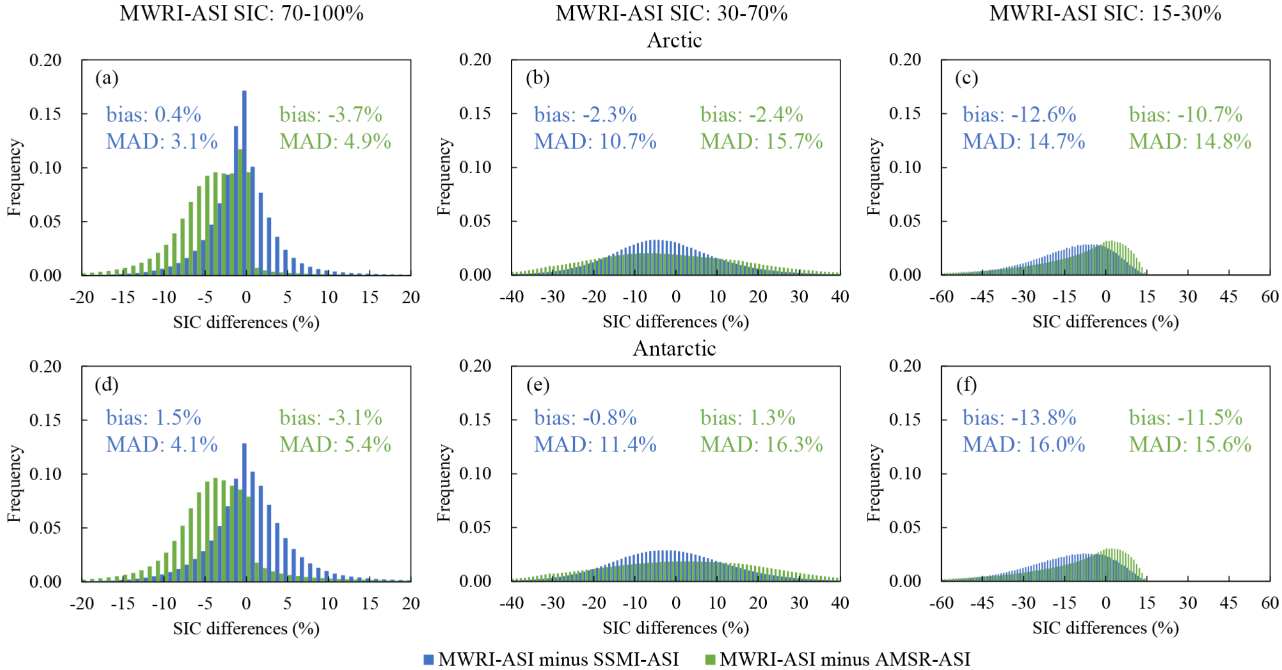

Figure 4: Histogram of SIC differences between the MWRI-ASI and SSMI-ASI and between the MWRI-ASI and AMSR-ASI with the MWRI-ASI SIC of 70–100%, 30–70%, and 15–30% from November 2010 to December 2019. Also shown are the differences in SIC between the MWRI-ASI and SSMI-ASI (blue number) and between the MWRI-ASI and AMSR-ASI (green number).

In the Arctic, in the freezing period of sea ice surface from late freeze onset to early melt onset, the SIC differences are lower with MAD of 2.7% between the MWRI-ASI and SSMI-ASI and of 4.5% between the MWRI-ASI and AMSR-ASI, respectively, compared to those (6.3% and 8.9%) in the surface melting period from melt onset to freeze onset. The MWRI-ASI SIC is higher than the SSMI-ASI SIC in the surface freezing stage but slightly smaller in the surface melting stage. These indicate that the differences among the ASI SIC products are larger in the surface melting state than in the surface freezing state and that the MWRI-ASI is more sensitive to melting ice surface than the SSMI-ASI.

3.2 Comparisons of the SIE products

In the Arctic, the MWRI-ASI SIE is smaller than the four existing SIE products of SSMI-NT, SSMI-BST, OSI-SAF, and Sea Ice Index, and has the smallest difference against the Sea Ice Index SIE with an overall MAD of 0.3×10^6 km^2 (Table 3). In the

https://doi.org/10.5194/essd-2022-186
Preprint. Discussion started: 16 September 2022

Antarctic, the MWRI-ASI SIE is larger than the Sea Ice Index SIE and lower than the other three SIE products, and it has the smallest differences against the Sea Ice Index SIE and OSI-SAF SIE, with an overall MAD of 0.2×10^6 km^2.

Table 3. Biases and MADs between the MWRI-ASI SIE and the four existing SIE products during the entire overlap periods, as well as the winter and summer months from December 2010 to December 2019. The underlined numbers represent the lowest biases and MADs.

		Overall (10^6 km^2)		Winter (10^6 km^2)		Summer (10^6 km^2)	
		bias	MAD	bias	MAD	bias	MAD
Arctic	SSMI-BST	-0.9	0.9	-0.9	0.9	-0.9	0.9
	SSMI-NT	-0.6	0.6	-0.7	0.7	-0.5	0.5
	OSI-SAF	-0.7	0.7	-0.7	0.7	-0.7	0.7
	Sea Ice Index	<u>-0.3</u>	<u>0.3</u>	<u>-0.5</u>	<u>0.5</u>	<u>-0.2</u>	<u>0.2</u>
Antarctic	SSMI-BST	-0.5	0.5	-0.3	0.3	-0.6	0.6
	SSMI-NT	-0.2	0.3	<0.1	0.2	-0.4	0.4
	OSI-SAF	<u>-0.2</u>	<u>0.2</u>	<u>-0.1</u>	<u>0.1</u>	-0.3	0.3
	Sea Ice Index	<u>0.2</u>	<u>0.2</u>	0.4	0.4	<u>0.1</u>	<u>0.1</u>

Table 4. Trends of the MWRI-ASI SIE and the four existing SIE products, and differences in trends between the MWRI-ASI SIE and the four existing SIE products from December 2010 to December 2019. Original trends of the four existing SIE products, combined trends (January 1979 to November 2010: four existing SIE products; December 2010 to December 2019: MWRI-ASI), and differences in trends between the original and combined SIEs from January 1979 to December 2019. The underlined numbers represent the lowest differences.

		12/2010 – 12/2019 (km^2 yr^{-1})		01/1979 – 12/2019 (km^2 yr^{-1})		
		Trend	Differences	Original trend	Combined trend	Differences
Arctic	MWRI-ASI	-49,214 ± 10,884**	-	-	-	-
	SSMI-BST	-58,279 ± 12,654**	9,065	-57,644 ± 1,511**	-80,653 ± 1,831**	-23,009
	SSMI-NT	-48,705 ± 12,672**	<u>-509</u>	-55,879 ± 1,504**	-70,205 ± 1,608**	-14,326
	OSI-SAF	-50,705 ± 11,529**	1,491	-53,379 ± 1,395**	-70,653 ± 1,567**	-17,274
	Sea Ice Index	-45,527 ± 12,229**	-3,687	-56,330 ± 1,489**	-64,673 ± 1,440**	<u>-8,343</u>
Antarctic	MWRI-ASI	-191,993 ± 25,790**	-	-	-	-
	SSMI-BST	-181,269 ± 25,942**	-10,724	6,057 ± 2,192**	-5,834 ± 2,400*	-11,891
	SSMI-NT	-178,209 ± 26,145**	-13,784	6,995 ± 2,189**	1,628 ± 2,305	-5,367
	OSI-SAF	-183,065 ± 25,547**	<u>-8,928</u>	9,567 ± 2,171**	4,831 ± 2,253*	<u>-4,736</u>
	Sea Ice Index	-176,685 ± 25,461**	-15,308	7,436 ± 2,138**	13,433 ± 2,192**	5,997

From 2010 to 2019, the MWRI-ASI SIE shows a significant decline trend of -49,214 km^2 yr^{-1} (P<0.01) in the Arctic and has the smallest difference in trends (-509 km^2 yr^{-1}) against the SSMI-NT SIE (Table 4). In the Antarctic, the largest decreasing trend is identified for the MWRI-ASI SIE (-191,993 km^2 yr^{-1}, P<0.01), and the difference in trends between the MWRI-ASI SIE and OSI-SAF SIE is the lowest (-8,928 km^2 yr^{-1}).

https://doi.org/10.5194/essd-2022-186
Preprint. Discussion started: 16 September 2022

In the period from 1979 to 2019, the four existing SIE products show significant decreasing trends (about -55,000 km^2 yr^{-1}, P<0.01) in the Arctic and increasing trends (about 7,500 km^2 yr^{-1}, P<0.01) in the Antarctic (Table 4). The decreasing trends (P<0.01) of the combined SIEs in the Arctic are larger (by 15% to 40%) than those of the original SIEs because the MWRI-ASI SIE is lower than the four existing SIEs from 2010 to 2019. For the combination of the Sea Ice Index SIE and MWRI-ASI SIE in the Arctic, the differences in trends between the original and combined SIEs are relatively small (-8,343 km^2 yr^{-1}) compared to other combinations. In the Antarctic, the relatively small increasing trend of the original SSMI-BST SIE is reversed by the SIE combination of the SSMI-BST and MWRI-ASI due to lower MWRI-ASI SIE. The trend combining the Sea Ice Index SIE and MWRI-ASI SIE (P<0.01) in the Antarctic is larger than the original Sea Ice Index SIE trend because the MWRI-ASI SIE is higher than the Sea Ice Index SIE from 2010 to 2019. The combined Antarctic SIE trend of the OSI-SAF and MWRI-ASI (P<0.05) has the lowest differences (-4,736 km^2 yr^{-1}) against the original OSI-SAF SIE trend, compared to other combined SIE trends. Seasonally, in the Arctic, the differences in trends between the original and combined SIEs are larger in winter than in summer, because the differences between the MWRI-ASI SIE and four existing SIEs are larger in winter than in summer when more coastal sea ice identified by the MWRI-ASI reduces the absolute deviations. In the Antarctic, the summer trends of the original SIEs are insignificant, but the winter increasing trends (P<0.05) are identified by all original SIEs and combined SIEs, except for the combination of the SSMI-BST SIE and MWRI-ASI SIE. Thereby, using the MWRI-ASI SIE instead of the original SIEs to construct a new time series has a greater impact on identifying the changing trend in SIE of the Antarctic than that of the Arctic because the Antarctic SIE trend is not as obvious as that of the Arctic.

For the Arctic annual maximum SIEs from 2011 to 2019, the ranking provided by the MWRI-ASI is the same as those provided by the SSMI-BST and Sea Ice Index, and all the largest values were observed in March 2012 for the five SIEs (Fig. 5). For the Arctic annual minimum SIEs, all the five SIEs identify the smallest and second-smallest values in September 2012 and 2019, respectively. The five SIEs have different rankings for 2013 and 2014 when the two largest Arctic annual minimum SIEs in 2011–2019 appeared, and the MWRI-ASI identifies the largest value in 2013, as the SSMI-BST and SSMI-NT. The five SIEs provide the same ranking of the Antarctic annual maximum SIEs and identify the largest and smallest SIEs in September 2014 and 2017, respectively, indicating the sudden drop after 2014 and rise after 2017 of Antarctic SIE can be depicted by all the five SIEs. The MWRI-ASI SIE reveals the smallest Antarctic annual minimum SIEs in 2017, as the SSMI-BST, OSI-SAF, and Sea Ice Index, but the SSMI-NT identifies the smallest value (2.4×10^6 km^2) in 2018, which is slightly smaller than those in 2017 by 0.005×10^6 km^2. The MWRI-ASI has the same ranking for the five largest Antarctic annual minimum SIEs as the SSMI-BST and SSMI-NT. Thereby, the MWRI-ASI SIE is reasonable for identifying the extreme cases of both the annual maximum and minimum SIEs in the bipolar regions, only with small differences appearing in some individual years with low SIE differences compared to other products.

https://doi.org/10.5194/essd-2022-186
Preprint. Discussion started: 16 September 2022

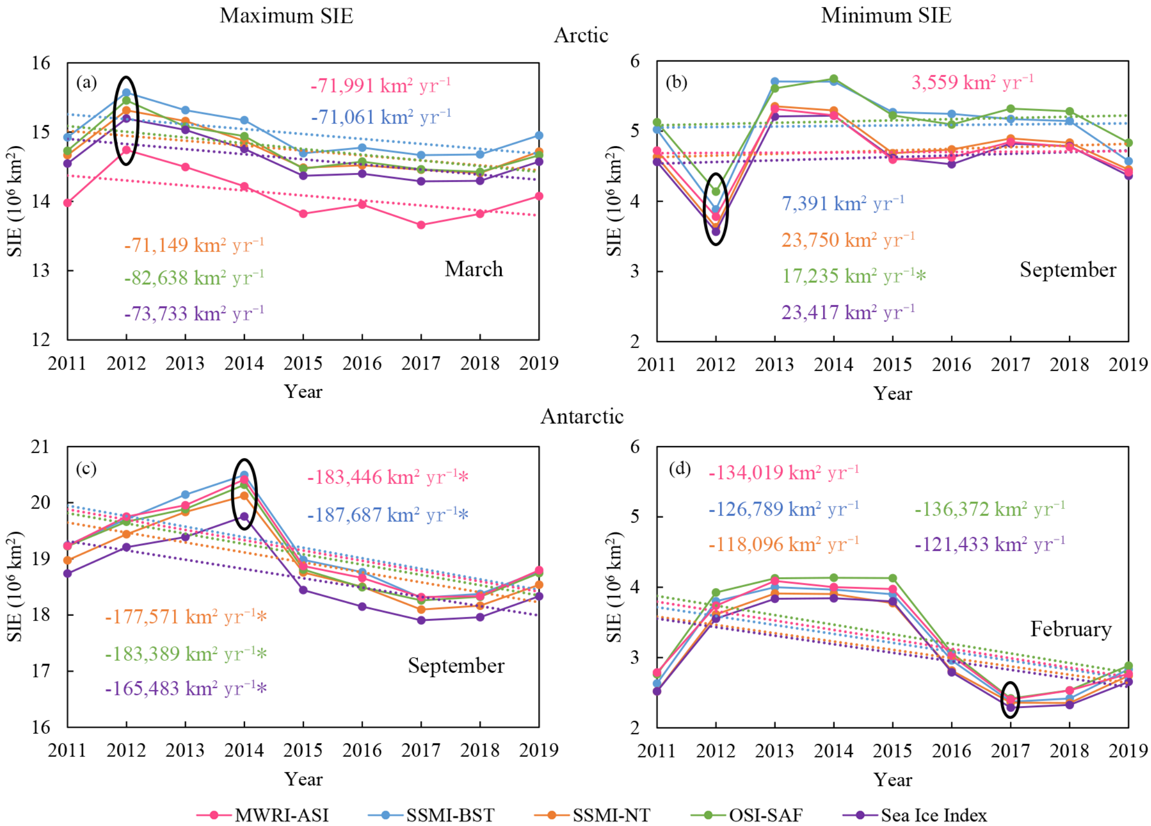

305

Figure 5: Annual maximum and minimum SIEs from 2011 to 2019. Also shown are the corresponding SIE trends of the MWRI-ASI (pink number), SSMI-BST (blue number), SSMI-NT (orange number), OSI-SAF (green number), and Sea Ice Index (purple number). The black circles present the largest annual maximum SIE and the smallest annual minimum SIE. Note that the smallest Antarctic annual minimum SIE of the SSMI-NT is observed in February 2018.

3.3 Comparisons to the ship-based SIC

The differences between the MWRI-ASI SIC and ship-based SIC are concentrated from -20% to 20%, generally accounting for 71% and 68% of the total samples in the Arctic and Antarctic, respectively (Fig. 6). In the region with high SIC (70–100%), about 82% of SIC differences between the MWRI-ASI and ship-based observation are distributed from -20% and 20%. However, this value decreases to about 67% and 46% in the regions with low SIC (15–30%) and medium SIC (30–70%), respectively. The MWRI-ASI SIC has smaller differences against the ship-based SIC in the regions with SIC above 70%, with MAD of 12.5% in the Arctic and of 12.3% in the Antarctic, respectively, compared to those (16.1% and 17.1%) obtained for all samples. It indicates the accuracy of the MWRI-ASI SIC is higher in the regions with high SIC than in the regions with low or medium SIC.

https://doi.org/10.5194/essd-2022-186
Preprint. Discussion started: 16 September 2022

Open Access Earth System Science Data Discussions

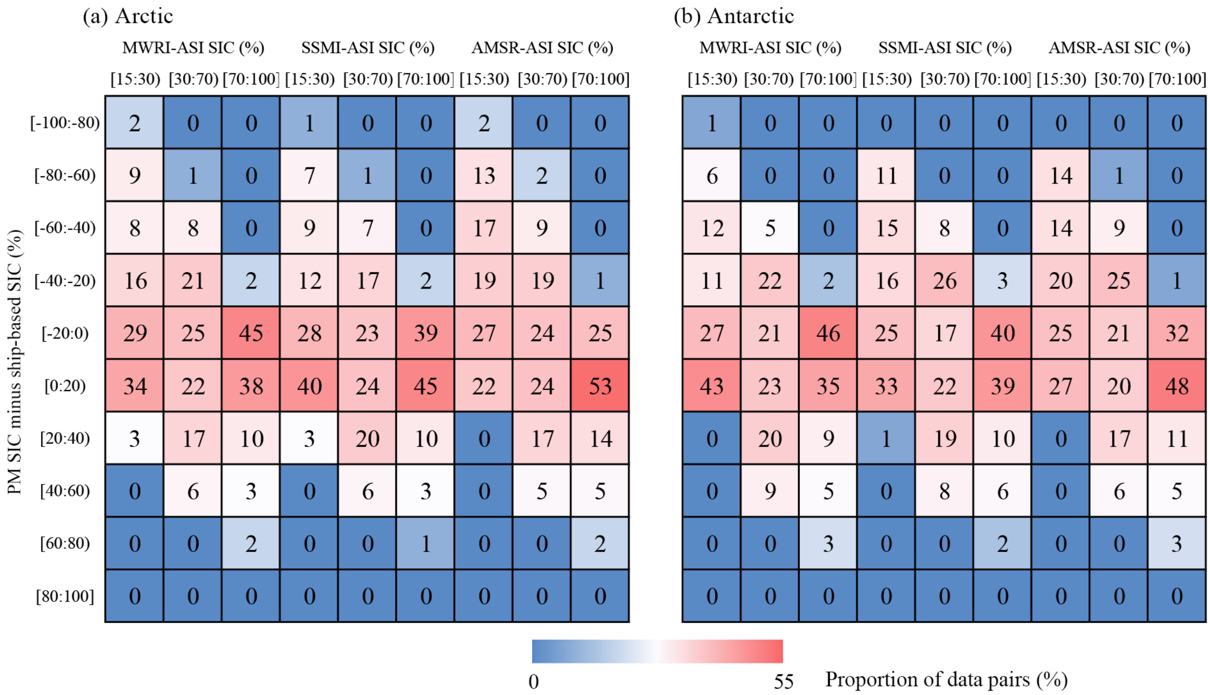

Figure 6: Proportion of data pairs (number in the grid) of the PM SIC products vs SIC differences between the PM SIC products and ship-based SIC. The PM SIC products are divided to 15–30%, 30–70%, and 70–100% (horizontal axis). The SIC differences are grouped with an interval of 20% from -100% to 100% (vertical axis).

Seasonally, in summer, the MADs between the MWRI-ASI SIC and ship-based SIC are 16.7% in the Arctic and 18.4% in the Antarctic, respectively, increasing by 5% and 4.8% compared to those in winter (Table 5). This implies that the MWRI-ASI SIC has a better accuracy in winter than in summer, which is due to the high sensitivity of PM signal to atmospheric and ice surface melting conditions.

Spatially (Fig. 7), the SIC differences between the MWRI-ASI and ship-based observations within 50 km away from the coast are larger with MAD of 23.1% in the Arctic and of 21.7% in the Antarctic, respectively, compared to those (15.8% and 16.2%) beyond 50 km away from the coast. It illustrates that the accuracy of the MWRI-ASI SIC can be affected by the coast to a slight degree. In general, the MWRI-ASI SIC has comparable accuracy with the SSMI-ASI SIC and AMSR-ASI SIC, when compared to the ship-based observations.

https://doi.org/10.5194/essd-2022-186
Preprint. Discussion started: 16 September 2022

Table 5. Biases, MADs. RMSDs, and *Rs* between the PM SIC products and ship-based SIC during the entire overlap periods, as well as the summer and winter months from 2010 to 2019. The 'Count' is the number of data pairs of the individual PM SIC and ship-based SIC.

		Arctic			Antarctic		
		MWRI-ASI	SSMI-ASI	AMSR-ASI	MWRI-ASI	SSMI-ASI	AMSR-ASI
Overall	Count	5230	5508	6169	2599	2613	2979
	bias (%)	1.6	2.5	5.9	3.3	1.4	4.1
	MAD (%)	16.1	15.5	16.3	17.1	18.2	16.5
	RMSD (%)	22.5	21.6	23.5	23.1	24.4	23.5
	R	0.60**	0.66**	0.57**	0.62**	0.57**	0.57**
Winter	Count	649	655	670	696	794	910
	bias (%)	-4.3	-3.8	-0.2	3.3	0.7	2.7
	MAD (%)	11.7	11.4	7.0	13.6	14.5	13.3
	RMSD (%)	18.9	17.9	14.8	19.1	19.8	19.9
	R	0.44**	0.53**	0.42**	0.67**	0.64**	0.58**
Summer	Count	4581	4853	5499	1903	1819	2069
	bias (%)	2.5	3.4	6.6	3.3	1.8	4.7
	MAD (%)	16.7	16.0	17.4	18.4	19.8	17.9
	RMSD (%)	23.0	22.1	24.3	24.5	26.2	24.9
	R	0.59**	0.66**	0.55**	0.59**	0.53**	0.56**

https://doi.org/10.5194/essd-2022-186
Preprint. Discussion started: 16 September 2022

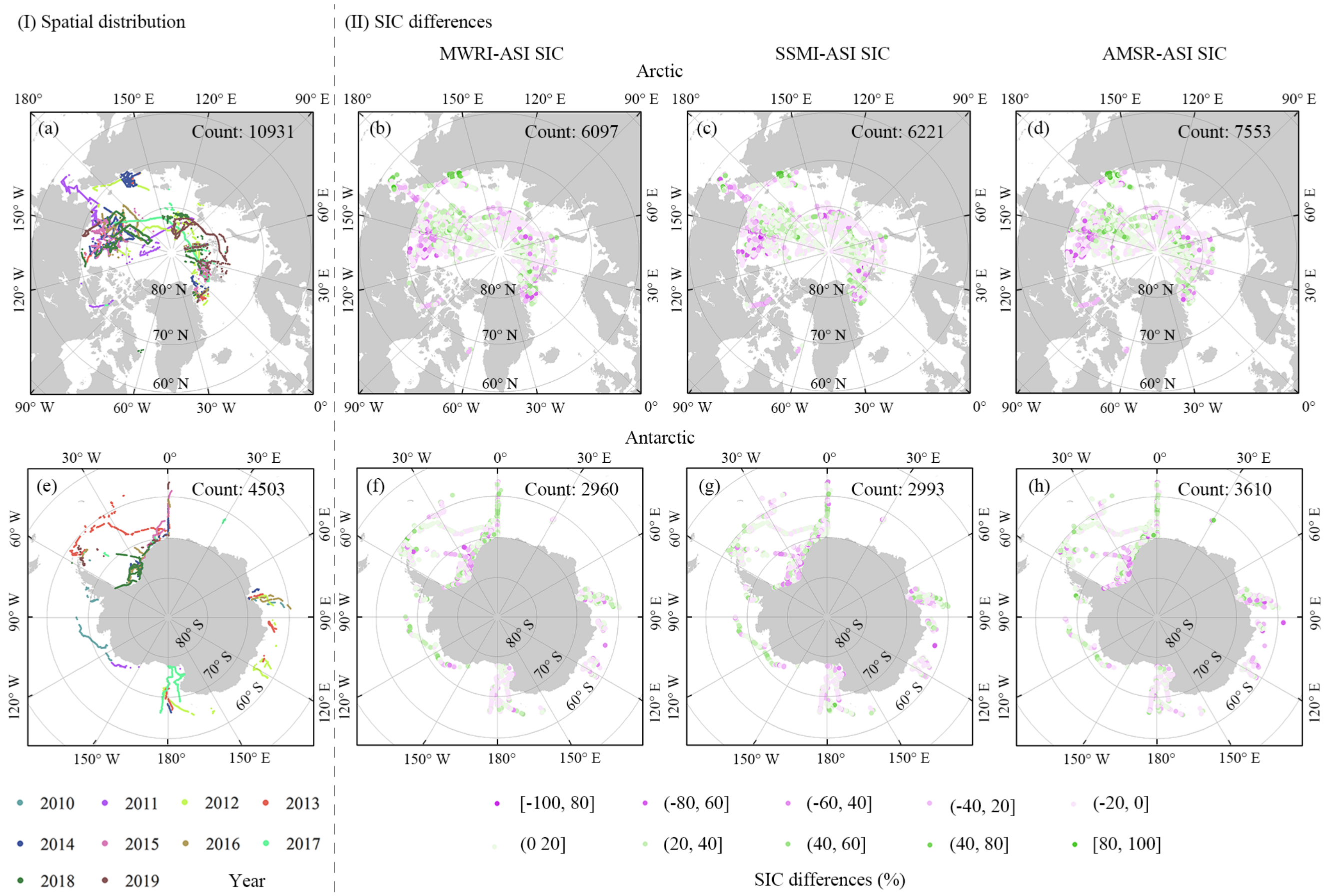

Figure 7: (I). Spatial distributions of the ship-based observational SIC in 2010–2019. (II). SIC differences between the PM SIC products and ship-based observations.

4 Discussion

4.1 Improvements and limitations of the MWRI-ASI v2 SIC

Compared to the preliminary version of MWRI-ASI SIC generated by Zhao et al. (2022) (MWRI-ASI v1 SIC), the MWRI-ASI SIC generated by this study (MWRI-ASI v2 SIC) is lower by -2.8% in the Arctic in 2018, especially in the MIZ and in summer. The MWRI-ASI v1 SIC was integrated into AMSR-ASI SIC, but the time series of AMSR-ASI is shorter than the SSMI-ASI SIC. To integrate the MWRI-ASI SIC into longer-term SIC products, this study modified the previous algorithm and adopted the SSMI-ASI SIC as referential SIC to update and extend the MWRI-ASI SIC, because it is vital to generate a consistent and continuous time series data for the studies of sea ice climate (Comiso and Nishio, 2008). The MWRI TB applied for the MWRI-ASI v1 SIC were just bias-corrected with the AMSR2 TB by a linear aggression during the one-year overlap period of 2018. As a result, the systematic deviations between the MWRI-ASI v1 SIC and

https://doi.org/10.5194/essd-2022-186
Preprint. Discussion started: 16 September 2022

AMSR-ASI SIC increased in 2019 compared to those in 2018, especially in summer (Chen et al., 2021). To obtain a more consistent SIC product, the re-calibrated MWRI TB were adopted as input source TB, because the biases among the re-calibrated MWRI TB were lower than those among the raw MWRI TB (Wu et al., 2022). From 2018 to 2019, when only the FY-3D MWRI TB were used, the differences in systematic deviations between the MWRI-ASI v2 SIC and AMSR-ASI SIC were 0.6% in summer, which were relatively small compared to those (1%) between the MWRI-ASI v1 SIC and AMSR-ASI SIC. It indicates that the consistency of the MWRI-ASI v2 SIC is improved compared with the MWRI-ASI v1 SIC.

However, the MWRI-ASI SIC v2 is still limited in terms of the land spillover and weather effects. Due to the differences in the size of the view field of different TB frequencies and the differences in observational TB of open water and land, the spurious sea ice would emerge in the PM observations along the coasts (Lavergne et al., 2019; Kern et al., 2019). Compared to the SSMI-ASI and AMSR-ASI, the MWRI-ASI reveals more ice along the coasts and around the islands, such as around 72° N from 138° E to 144° E in the Arctic and around 78° S from 160° W to 170° E in the Antarctic (Fig. 8). The ice along the coast extends about two grids (25 km) from the coastline, leading to the overestimation of the MWRI-ASI SIE in summer compared to the SSMI-ASI SIE.

The spurious sea ice over open water arises from the atmospheric effect, i.e., water vapor, cloud liquid water, surface winds, and precipitation (Kern, 2004). Although the methods to remove the spurious ice have been applied, some spurious floes remain and some small real floes are ignored in the MIZ. The MWRI-ASI weather filters can remove most of the spurious ice (Fig, 8). However, after applying the weather filters, more ice floes have been identified by the MWRI-ASI in the MIZ compared to the SSMI-ASI and AMSR-ASI. It is difficult to determine whether this residual ice is erroneous ice caused by weather effects or the real discrete small ice floes. Thus, in the next step, we attempt to identify and remove the spurious ice caused by land spillover and weather effects, by using the optical or synthetic aperture radar images with higher resolutions, to further improve our MWRI-ASI SIC product.

https://doi.org/10.5194/essd-2022-186
Preprint. Discussion started: 16 September 2022

Open Access Earth System Science Data Discussions

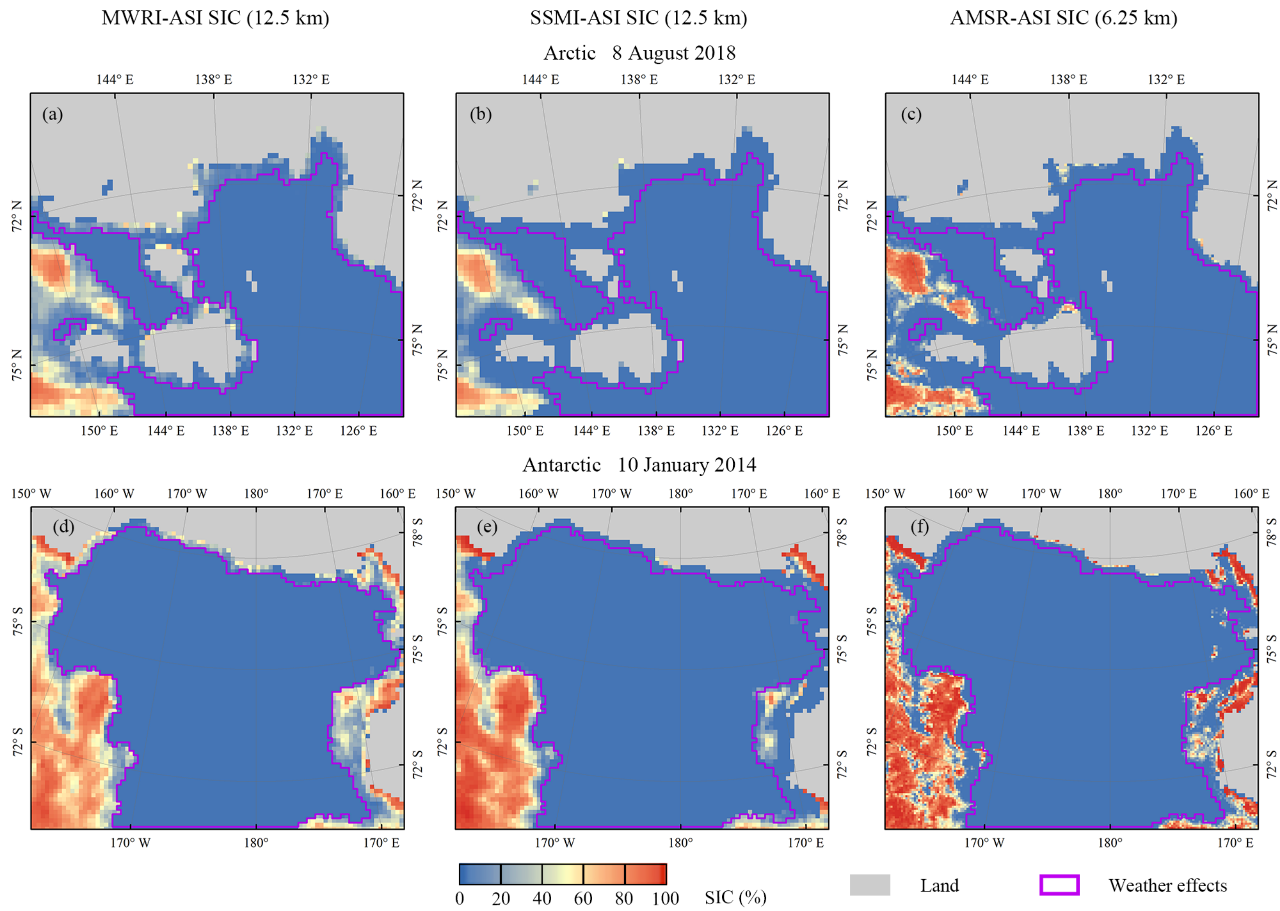

Figure 8: SIC distributions of the MWRI-ASI, SSMI-ASI, and AMSR-ASI in the coastal MIZ. Also shown are the weather-affected grids removed by the MWRI-ASI weather filters.

4.2 Comparisons to prior studies on SIC products in the polar regions

The biases between our MWRI-ASI SIE and Sea Ice Index SIE from 2015 to 2017 are -0.3×10^6 km^2 in the Arctic and 0.2×10^6 km^2 in the Antarctic, respectively, which are within the range of SIE biases in the same period shown in Meier and Stewart (2019). Seasonally, in the bipolar regions, our MWRI-ASI SIE has larger absolute deviations against the Sea Ice Index SIE in winter than in summer. The absolute deviation of Arctic SIE reduces in summer because our MWRI-ASI SIE has been involved more sea ice along the coastline and at the ice edge in summer than in winter. In the Antarctic, our MWRI-ASI SIE is about two grids (25 km) farther south than the Sea Ice Index SIE, and the absolute deviation increases in winter because the SIE is larger in winter than in summer. The seasonal variation pattern of biases between our MWRI-ASI SIE and Sea Ice Index SIE is similar to those between the AMSR-BST SIE and Sea Ice Index SIE in the Arctic (Meier and Stewart, 2019).

Beitsch et al. (2015) revealed that the accuracies of the AMSR-E ASI SIC and SSMI-ASI SIC are consistent, with overall RMSDs of about 13% compared to the ASPeCt observations from 2002 to 2010. Our study also indicates that the accuracy of

https://doi.org/10.5194/essd-2022-186
Preprint. Discussion started: 16 September 2022

the MWRI-ASI SIC is comparable to those of the SSMI-ASI SIC and AMSR-ASI SIC, with overall RMSDs of about 23% compared to the Ice Watch/ASSIST and ASPeCt observations from 2010 to 2019. The accuracy of our MWRI-ASI SIC is lower in summer than in winter, which is consistent with those of the AMSR-E ASI SIC and SSMI-ASI SIC (Beitsch et al., 2015).

5 Data availability

The SIC product derived from the FY-3 MWRI sensors can be downloaded from the data repositories PANGAEA at https://doi.pangaea.de/10.1594/PANGAEA.945188 (Chen et al., 2022). This dataset is available from 12 November 2010 to 31 December 2019 with temporary data gaps of 23 days in the Arctic and 82 days in the Antarctic. The SIC files are named "FY_MWRI_SIC_DAILY_YYYYMMDD_Region.tif", with "YYYYMMDD" denoting the date and "Region" representing the Arctic or Antarctic. This SIC dataset is archived in TIFF format, which can be read with Python, ENVI/IDL, and MATLAB software. The values '0-100' are the percentage of SIC, '-1' is the land, '-2' is the Pole Hole, and 'NoData' is the missing data. Besides, the biases between this SIC dataset and other two ASI SIC products, i.e., SSMI-ASI and AMSR-ASI, are provided.

6 Conclusion

This study generates a new SIC product in the polar regions from November 2010 to December 2019, which is derived from the recent re-calibrated TB data of the MWRI sensors onboard the FY-3B, FY-3C, and FY-3D satellites using the modified dynamic tie points ASI algorithm. Generally, the MWRI-ASI SIC or SIE can reasonably identify the seasonal and long-term changes of sea ice, as well as the extreme cases of annual maximum/minimum SIE for both the Arctic and Antarctic.

To test the ability of the MWRI-ASI as an important complement of the existing PM SIC or SIE records, the MWRI-ASI SIC is compared to the existing ASI SIC products of SSMI-ASI and AMSR-ASI, and the MWRI-ASI SIE is compared to the existing SIE products of SSMI-BST, SSMI-NT, OSI-SAF, and Sea Ice Index. The accuracy of the MWRI-ASI is also validated using the ship-based observed SIC.

Both the daily SIC and SIE derived from the MWRI-ASI closely agree with those derived from the SSMI-ASI, with overall SIC biases of -1.4% and 0.5%, and with overall SIE biases of 0.1×10^6 km^2 and -0.02×10^6 km^2 in the Arctic and Antarctic, respectively. The ability of the MWRI-ASI to observe the sea ice in the MIZ mostly coincides with that of the SSMI-ASI. Therefore, the MWRI-ASI SIC is the most appropriate backup for the SSMI-ASI SIC. However, compared with the SSMI-ASI SIC, the sensitivity of MWRI-ASI SIC to sea ice melting surface is higher, which can be reduced by analyzing the characteristic of sea ice surface melting at 89 GHz of the MWRI TB in future work.

The MWRI-ASI SIE can be better integrated into the Sea Ice Index SIE in the Arctic and the OSI-SAF SIE in the Antarctic compared to other products. This suggests the new MWRI-ASI SIC product can reduce the potential breaking risk of PM sea ice observations.

https://doi.org/10.5194/essd-2022-186
Preprint. Discussion started: 16 September 2022

The MWRI-ASI SIC has a higher accuracy in winter and in the regions with high SIC than in summer and in the regions with low or medium SIC. Based on the comparison with the ship-based observations, the accuracy of the MWRI-ASI SIC is comparable to those of the SSMI-ASI SIC and AMSR-ASI SIC.

In the next work, we will attempt to identify and remove the spurious sea ice caused by land spillover and weather effects more accurately by using satellite-based observations with higher resolutions to further improve the MWRI-ASI SIC. In addition, based on the re-calibrated TB data of the MWRI sensors, we can produce other sea ice parameters in the polar regions, e.g., lead area fraction, onsets of ice surface melt or freeze, and polynya area.

Author Contributions.

YC performed the experiments and wrote the manuscript. XP and XZ provided the conception of the study and suggestions on manuscript. RL contributed to the manuscript revision, results analysis, and discussions. SW and PZ provided valuable instructions on data and methods. YL, PF, and QJ advised on the model code. All authors contributed to the improvement of the manuscript.

Competing interests.

The authors declare that they have no conflict of interest.

Acknowledgements.

We would like to acknowledge the organizations that shared their datasets for use in this study. The Chinese National Satellite Meteorological Center provided the re-calibrated MWRI TB dataset. The Polar Research Institute of China provided the ship-based observational SIC. The Integrated Climate Data Center (ICDC) of the University of Hamburg provided the SSMI-ASI SIC product and ESA-CCI ship-based observed SIC. The Institute of Environmental Physics of the University of Bremen provided the AMSR2-ASI SIC product. The U.S. Geological Survey (USGS), NASA National Snow and Ice Data Center provided the SSMI-BST, SSMI-NT, and Sea Ice Index SIE datasets. The Exploitation of Meteorological Satellites (EUMETSAT) Ocean and Sea Ice Satellite Application Facility (OSI-SAF) provided the OSI-SAF SIE datasets. The U.S. Geological Survey (USGS), NASA Goddard Earth Science Projects provided the Arctic sea ice surface melt/freeze onset data. We also want to acknowledge the contributors of the ship-based observed SIC in the IceWatch and PANGAEA databases.

Financial support.

This work was supported by the National Key Research and Development Program of China (grant Nos. 2018YFA0605903, 2021YFC2801304, and 2018YFB0504905), the National Natural Science Foundation of China (grant Nos. 42076235 and 41876223), and the Fundamental Research Funds for the Central Universities (grant No. 2042022kf0018).

References

Beitsch, A., Kern, S., and Kaleschke, L.: Comparison of SSM/I and AMSR-E sea ice concentrations with ASPeCt ship observations around Antarctica, IEEE Trans. Geosci. Remote Sens., 53, 1985–1996, https://doi.org/10.1109/TGRS.2014.2351497, 2015.

Cavalieri, D. J., St Germain, K. M., and Swift, C. T.: Reduction of weather effects in the calculation of sea-ice concentration with the DMSP SSM/I, J. Glaciol., 41, 455–464, https://doi.org/10.1017/S0022143000034791, 1995.

Chen, Y., Zhao, X., Pang, X., and Ji, Q.: Daily sea ice concentration product based on brightness temperature data of FY-3D MWRI in the Arctic, Big Earth Data, 00, 1–15, https://doi.org/10.1080/20964471.2020.1865623, 2021.

Chen, Y., Pang, X., Lei, R., and Zhao, X.: Sea ice concentration derived from temperature brightness data of the Microwave Radiation Imager sensors onboard the Chinese FengYun-3 satellites in the polar regions from 2010 to 2019, https://doi.org/https://doi.pangaea.de/10.1594/PANGAEA.945188, 2022.

Comiso, J. C. and Nishio, F.: Trends in the sea ice cover using enhanced and compatible AMSR-E, SSM/I, and SMMR data, J. Geophys. Res. Ocean., 113, 1–22, https://doi.org/10.1029/2007JC004257, 2008.

Comiso, J. C., Cavalieri, D. J., and Markus, T.: Sea ice concentration, ice temperature, and snow depth using AMSR-E data, IEEE Trans. Geosci. Remote Sens., 41, 243–252, https://doi.org/10.1109/TGRS.2002.808317, 2003.

Comiso, J. C., Meier, W. N., and Gersten, R.: Variability and trends in the Arctic Sea ice cover: Results from different techniques, J. Geophys. Res. Ocean., 122, 6883–6900, https://doi.org/10.1002/2017JC012768, 2017.

Eisenman, I., Meier, W. N., and Norris, J. R.: A spurious jump in the satellite record: Has Antarctic sea ice expansion been overestimated?, 8, 1289–1296, https://doi.org/10.5194/tc-8-1289-2014, 2014.

Fetterer, F., Knowles, K., Meier, W. N., Savoie, M. H., and Windnagel, A. K.: updated daily. Sea Ice Index, Version 3. [Monthly Sea Ice Extent], Boulder, Color. USA. NSIDC Natl. Snow Ice Data Center., https://doi.org/10.7265/N5K072F8, 2017.

Gerland, S., Barber, D., Meier, W., Mundy, C. J., Holland, M., Kern, S., Li, Z., Michel, C., Perovich, D. K., and Tamura, T.: Essential gaps and uncertainties in the understanding of the roles and functions of Arctic sea ice, Environ. Res. Lett., 14, https://doi.org/10.1088/1748-9326/ab09b3, 2019.

Gloersen, P. and Cavalieri, D. J.: Reduction of weather effects in the calculation of sea ice concentration from microwave radiances, J. Geophys. Res., 91, 3913, https://doi.org/10.1029/jc091ic03p03913, 1986.

https://doi.org/10.5194/essd-2022-186
Preprint. Discussion started: 16 September 2022

Heil, P., Fowler, C. W., and Lake, S. E.: Antarctic sea-ice velocity as derived from SSM/I imagery, Ann. Glaciol., 44, 361–366, https://doi.org/10.3189/172756406781811682, 2006.

Hutchings, J., Delamere, J., and Heil, P.: The Ice Watch Manual, 2019.

Ivanova, N., Pedersen, L. T., Tonboe, R. T., Kern, S., Heygster, G., Lavergne, T., Sørensen, A., Saldo, R., Dybkjær, G., Brucker, L., and Shokr, M.: Inter-comparison and evaluation of sea ice algorithms: Towards further identification of challenges and optimal approach using passive microwave observations, 9, 1797–1817, https://doi.org/10.5194/tc-9-1797-2015, 2015.

Jiménez, C., Tenerelli, J., Prigent, C., Kilic, L., Lavergne, T., Skarpalezos, S., Høyer, J. L., Reul, N., and Donlon, C.: Ocean and Sea Ice Retrievals From an End-To-End Simulation of the Copernicus Imaging Microwave Radiometer (CIMR) 1.4–36.5 GHz Measurements, J. Geophys. Res. Ocean., 126, 1–23, https://doi.org/10.1029/2021JC017610, 2021.

Kaleschke, L., Lüpkes, C., Vihma, T., Haarpaintner, J., Bochert, A., Hartmann, J., and Heygster, G.: SSM/I sea ice remote sensing for mesoscale ocean-atmosphere interaction analysis, Can. J. Remote Sens., 27, 526–537, https://doi.org/10.1080/07038992.2001.10854892, 2001.

Kern, S.: A new method for medium-resolution sea ice analysis using weather-influence corrected Special Sensor Microwave/Imager 85 GHz data, Int. J. Remote Sens., 25, 4555–4582, https://doi.org/10.1080/01431160410001698898, 2004.

Kern, S.: ESA-CCI_Phase2_Standardized_Manual_Visual_Ship-Based_SeaIceObservations_v02, World Data Cent. Clim. DKRZ, https://doi.org/10.26050/WDCC/ESACCIPSMVSBSIOV2, 2019.

Kern, S., Lavergne, T., Notz, D., Toudal Pedersen, L., Tage Tonboe, R., Saldo, R., and Macdonald Sørensen, A.: Satellite passive microwave sea-ice concentration data set intercomparison: Closed ice and ship-based observations, 13, 3261–3307, https://doi.org/10.5194/tc-13-3261-2019, 2019.

Kern, S., Kaleschke, L., Girard-Ardhuin, F., Spreen, G., and Beitsch, A.: Global daily gridded 5-day median-filtered, gap-filled ASI Algorithm SSMI-SSMIS sea ice concentration data, Integr. Clim. Date Cent. (ICDC), CEN, Univ. Hamburg, Ger., https://www.cen.uni-hamburg.de/en/icdc/data/cryosphere/seaiceconcentration-asi-ssmi.html 2020.

Lavergne, T., Macdonald Sørensen, A., Kern, S., Tonboe, R., Notz, D., Aaboe, S., Bell, L., Dybkjær, G., Eastwood, S., Gabarro, C., Heygster, G., Anne Killie, M., Brandt Kreiner, M., Lavelle, J., Saldo, R., Sandven, S., and Pedersen, L. T.: Version 2 of the EUMETSAT OSI SAF and ESA CCI sea-ice concentration climate data records, 13, 49–78, https://doi.org/10.5194/tc-13-49-2019, 2019.

Lavergne, T., Aaboe, S., Neuville, A., Macdonald Sørensen, A., and Eastwood, S.: Product User Manual for the Sea Ice Index, version 2.1, 1–18, 2020.

Lavergne, T., Kern, S., Aaboe, S., Derby, L., Dybkjaer, G., Garric, G., Heil, P., Hendricks, S., Holfort, J., Howell, S., Key, J., Lieser, J. L., Maksym, T., Maslowski, W., Meier, W., Munoz-Sabater, J., Nicolas, J., Özsoy, B., Rabe, B., Rack, W., Raphael, M., de Rosnay, P., Smolyanitsky, V., Tietsche, S., Ukita, J., Vichi, M., Wagner, P., Willmes, S., and Zhao, X.: A New Structure for the Sea Ice Essential Climate Variables of the Global Climate Observing System, Bull. Am. Meteorol. Soc., 1–41, https://doi.org/10.1175/bams-d-21-0227.1, 2022.

Lei, R., Tian-Kunze, X., Li, B., Heil, P., Wang, J., Zeng, J., and Tian, Z.: Characterization of summer Arctic sea ice morphology in the 135°-175°W sector using multi-scale methods, Cold Reg. Sci. Technol., 133, 108–120, https://doi.org/10.1016/j.coldregions.2016.10.009, 2017.

Markus, T., Stroeve, J. C., and Miller, J.: Recent changes in Arctic sea ice melt onset, freezeup, and melt season length, J. Geophys. Res. Ocean., 114, 1–14, https://doi.org/10.1029/2009JC005436, 2009.

Meier, W. N.: Satellite passive microwave observations of sea ice, 3rd ed., Elsevier Inc., 402–414 pp., https://doi.org/10.1016/B978-0-12-409548-9.11461-7, 2019.

Meier, W. N. and Ivanoff, A.: Intercalibration of AMSR2 NASA Team 2 Algorithm Sea Ice Concentrations with AMSR-E Slow Rotation Data, IEEE J. Sel. Top. Appl. Earth Obs. Remote Sens., 10, 3923–3933, https://doi.org/10.1109/JSTARS.2017.2719624, 2017.

Meier, W. N. and Stewart, J. S.: Assessing uncertainties in sea ice extent climate indicators, Environ. Res. Lett., 14, https://doi.org/10.1088/1748-9326/aaf52c, 2019.

Melsheimer, C. and Spreen, G.: AMSR-E/AMSR2 ASI sea ice concentration data,Arctic, Antarctica version 5.4 (NetCDF), https://doi.org/10.1594/PANGAEA.898400, 2020.

Newell, D., Draper, D., Remund, Q., Woods, B., Mays, C., Bensler, B., Miller, D., and Eastman, K.: Weather Satellite Follow-On–Microwave (WSF-M) design and predicted performance, Ball Aerospace, Boulder, Color. USA, 2020.

Parkinson, C. L. and DiGirolamo, N. E.: Sea ice extents continue to set new records: Arctic, Antarctic, and global results, Remote Sens. Environ., 267, 112753, https://doi.org/10.1016/j.rse.2021.112753, 2021.

Spreen, G., Kaleschke, L., and Heygster, G.: Sea ice remote sensing using AMSR-E 89-GHz channels, J. Geophys. Res. Ocean., 113, 1–14, https://doi.org/10.1029/2005JC003384, 2008.

Stroeve, J. and Meier, W. N.: Sea Ice Trends and Climatologies from SMMR and SSM/I-SSMIS, Version 3. Monthly total Sea Ice Extent Data, Boulder, Color. USA. NASA Natl. Snow Ice Data Cent. Distrib. Act. Arch. Center., https://doi.org/10.5067/IJ0T7HFHB9Y6, 2018.

Trewin, B., Cazenave, A., Howell, S., Huss, M., Isensee, K., Palmer, M. D., Tarasova, O., and Vermeulen, A.: Headline indicators for global climate monitoring, Bull. Am. Meteorol. Soc., 102, E20–E37, https://doi.org/10.1175/BAMS-D-19-0196.1, 2021.

Witze, A.: Ageing satellites put crucial sea-ice climate record at risk, Nature, 551, 13–14, https://doi.org/10.1038/nature.2017.22907, 2017.

Worby, A. P. and Allison, I.: A ship-based technique for observing Antarctic sea ice. Part I: Observational techniques and results, 1999.

Wu, S. and Liu, J.: Comparison of Arctic sea ice concentration datasets, Acta Ocean. Sin, 40, 64–72, https://doi.org/10.3969/j.issn.0253-4193.2018.11.007, 2018.

Wu, S., Sun, L., and Lu, Q.: An Independent Fundamental Climate Data Record From Ten-years, under Rev., 2022.

https://doi.org/10.5194/essd-2022-186
Preprint. Discussion started: 16 September 2022

Open Access Earth System Science Data Discussions

Xian, D., Zhang, P., Gao, L., Sun, R., Zhang, H., and Jia, X.: Fengyun Meteorological Satellite Products for Earth System Science Applications, Adv. Atmos. Sci., 38, 1267–1284, https://doi.org/10.1007/s00376-021-0425-3, 2021.

Xie, H., Lei, R., Ke, C., Wang, H., Li, Z., Zhao, J., and Ackley, S. F.: Summer sea ice characteristics and morphology in the Pacific Arctic sector as observed during the CHINARE 2010 cruise, 7, 1057–1072, https://doi.org/10.5194/tc-7-1057-2013, 2013.

Zhang, P., Chen, L., Xian, D., Zhe, X., Peng, Z., Lin, C., and Di, X.: Recent progress of Fengyun meteorology satellites, Chin. J. Sp. Sci, 38, 788–796, https://doi.org/10.11728/cjss2018.05.788, 2018.

Zhang, P., Lu, Q., Hu, X., Gu, S., Yang, L., Min, M., Chen, L., Xu, N., Sun, L., Bai, W., Ma, G., and Xian, D.: Latest Progress of the Chinese Meteorological Satellite Program and Core Data Processing Technologies, Adv. Atmos. Sci., 36, 1027–1045, https://doi.org/10.1007/s00376-019-8215-x, 2019.

Zhao, X., Chen, Y., Kern, S., Qu, M., Ji, Q., Fan, P., and Liu, Y.: Sea Ice Concentration Derived from FY-3D MWRI and Its Accuracy Assessment, IEEE Trans. Geosci. Remote Sens., 60, https://doi.org/10.1109/TGRS.2021.3063272, 2022.